'96 대한전기학회 하계학술대회 논문집 (1996. 7. 22~24)

공진형 직류 링크단을 이용한 유도전동기의 예측형 전류 제어

°오인환, 문건우, 김성권*, 윤명중
한국과학기술원 전기및전자공학과, *삼성전자 생산기술센타 자동화연구소

A Novel Predictive Current Control of Induction Motor Using Resonant DC Link Inverter

In-Hwan Oh, Gun-Woo Moon, *Sungkwun Kim, Myung-Joong Youn
Dept. of Electrical Engineering KAIST, *FA Research Institute Prod. Eng. Center SamSung Electronics

ABSTRACT **- A predictive current control technique for an induction motor employing a resonant DC link inverter is proposed to overcome the disadvantage of the current regulated delta modulation (CRDM) which was employed to control the resonant DC link inverter. The discrete model of an induction motor and estimation of back EMF are investigated and a novel predictive current control technique is newly developed based on this discrete model and estimated back EMF. Using the proposed control technique, the minimized current ripple with reduced offset can be obtained. The usefulness of the proposed technique is verified through the computer simulation.**

I. INTRODUCTION

Recently, a great deal of researches on the soft switching DC link inverter has been studied due to increasing demands for the high frequency and high efficiency operations of an induction motor drive system [1-4]. Among them, the actively clamped resonant DC link (ACRDCL) inverter offers a most practical and reliable way of reducing commutation losses and eliminating individual snubbers, thus allowing high operating frequencies and improved efficiency. The RDCL inverter employs the resonant LC tank in the DC link side to achieve a zero-voltage switching (ZVS) which allows much higher switching frequencies.

However, there exist some inherent disadvantages such as the relatively large current ripple and offset caused by a fixed intervals of the control cycle. Therefore, a novel predictive current control technique based on the space vector modulation is proposed in this paper as a new effective way of overcoming the disadvantages of the RDCL inverter based current control of an induction motor. To control the motor current with reduced ripple and offset, the information on the motor parameters should be considered to choose the optimal vector. This implies that the current prediction in the next time event can be obtained by using the exact discrete model of an induction motor. Based on this current prediction, the optimal voltage vector minimizing the present current error is analytically calculated to apply the actual voltage vector. Using the proposed control technique, near optimum inverter voltages with respect to the current ripple are obtained. Furthermore, a current offset is also notably reduced. Thus, the current ripple can be minimized and the high performance of the torque and speed controls can also be available by the precise motor current control. The proposed current control technique is compared with other types of current control techniques.

II. INDUCTION MOTOR MODELING

Based on the reference-frame theory, the state space model of a squirrel cage induction motor in a synchronous reference frame can be expressed as follows [7]:

$$\begin{bmatrix} \dot{\mathbf{i}}_s \\ \dot{\Psi}_r \end{bmatrix} = \begin{bmatrix} \mathbf{a}_{11} & \mathbf{a}_{12} \\ \mathbf{a}_{21} & \mathbf{a}_{22} \end{bmatrix} \begin{bmatrix} \mathbf{i}_s \\ \Psi_r \end{bmatrix} + \begin{bmatrix} \mathbf{b}_0 \\ \mathbf{0} \end{bmatrix} \mathbf{v}_s . \tag{1}$$

where $\mathbf{i}_s = [i_{ds} \quad i_{qs}]^T$, $\Psi_r = [\lambda_{dr} \quad \lambda_{qr}]^T$, and $\mathbf{v}_s = [v_{ds} \quad v_{qs}]^T$.

Also, each element of the system matrix can be expressed as follows :

$$\mathbf{a}_{11} = -\left[\frac{1}{\sigma\tau_s} + \frac{(1-\sigma)}{\sigma\tau_r}\right]\mathbf{I} - \omega_e \mathbf{J}, \qquad \mathbf{a}_{12} = \frac{L_m}{\sigma L_s L_r}\left[\frac{1}{\tau_r}\mathbf{I} - \omega_r \mathbf{J}\right]$$

$$\mathbf{a}_{21} = \left[\frac{L_m}{\tau_r}\right]\mathbf{I}, \qquad \mathbf{a}_{22} = -\left[\frac{1}{\tau_r}\right]\mathbf{I} + (\omega_e - \omega_r)\mathbf{J}$$

$$\mathbf{b}_0 = \frac{1}{\sigma L_s}\mathbf{I}, \quad \sigma = 1 - \frac{L_m^2}{L_s L_r}, \quad \mathbf{I} = \begin{bmatrix} 1 & 0 \\ 0 & 1 \end{bmatrix}, \quad \mathbf{J} = \begin{bmatrix} 0 & -1 \\ 1 & 0 \end{bmatrix}.$$

III. ROTOR FLUX OBSERVER

The information on the rotor flux is required to get the field oriented control. However, it is difficult to measure directly this flux so that the observer is used. From (1), the estimated rotor flux $\hat{\Psi}_r$ can be derived as

$$\begin{aligned} \dot{\hat{\Psi}}_r &= \mathbf{a}_{21}\mathbf{i}_s + \mathbf{a}_{22}\hat{\Psi}_r \\ &\quad + \mathbf{G}[\dot{\mathbf{i}}_s - (\mathbf{a}_{11}\mathbf{i}_s + \mathbf{a}_{12}\hat{\Psi}_r + \mathbf{b}_0\mathbf{v}_s)] \\ &= (\mathbf{a}_{22} - \mathbf{G}\mathbf{a}_{12})\hat{\Psi}_r \\ &\quad + (\mathbf{a}_{21} - \mathbf{G}\mathbf{a}_{11})\mathbf{i}_s - \mathbf{G}\mathbf{b}_0\mathbf{v}_s + \mathbf{G}\dot{\mathbf{i}}_s \end{aligned} \tag{2}$$

$$\dot{\mathbf{e}} = (\mathbf{a}_{22} - \mathbf{G}\mathbf{a}_{12})\mathbf{e} \tag{3}$$

where $\mathbf{G}$ is the observer gain and $\mathbf{e} = \hat{\Psi}_r - \Psi_r$. The block diagram is shown in Fig. 1. In case of no parameter variations, the dynamics of the estimation error can be represented as (3). If the system given by (3) is observable, the observer poles can be

assigned any desired locations by selecting the observer gain G appropriately. The magnitude of the rotor flux $\hat{\lambda}_r$ can be given from the flux observer as

$$\hat{\lambda}_r = \sqrt{(\hat{\lambda}_{dr}^2 + \hat{\lambda}_{qr}^2)} . \quad (4)$$

IV. PROPOSED PREDICTIVE CURRENT CONTROL SCHEME

It is considered that the desired control performance can be obtained by selecting each voltage vector in such a way that the present current error is reduced to be a minimum at the next time event. The equivalent circuits of an induction motor is shown in Fig. 5. In this figure, all parameters are converted into the stator side and $\mathbf{e}_s(t)$ denotes a counter EMF. From (1), the voltage equation can be written in terms of d-q voltages and counter EMF in a stationary frame as follows :

$$\mathbf{v}_s(t) = R_s \mathbf{i}_s(t) + \sigma L_s \frac{d\mathbf{i}_s(t)}{dt} + \frac{L_m}{L_r}\frac{d\Psi_r}{dt} . \quad (5)$$

It is desirable to use the estimated rotor flux $\hat{\Psi}_r$ because of difficulty in measuring the rotor flux Ψ_r directly. Therefore, the voltage equation of an induction motor can be written by using the estimated counter EMF as follows :

$$\hat{\mathbf{v}}_s(t) = R_s \mathbf{i}_s(t) + \sigma L_s \frac{d\mathbf{i}_s(t)}{dt} + \hat{\mathbf{e}}_s(t) \quad (6)$$

where $\hat{\mathbf{e}}_s(t) = \frac{L_m}{L_r}\frac{d\hat{\Psi}_r}{dt}$. The estimated values of counter EMF $\hat{\mathbf{e}}_s(t) = [\hat{e}_d(t) \quad \hat{e}_q(t)]^T$ can be obtained using the rotor flux calculated from the flux observer. Assuming the current $\mathbf{i}_s(t)$ to be constant during a sampling period, a discrete model of an induction motor is obtained from (6) as

$$\hat{\mathbf{v}}_s(k) = R_s \mathbf{i}_s(k) + \sigma L_s \frac{[\mathbf{i}_s(k+1) - \mathbf{i}_s(k)]}{t_s} + \hat{\mathbf{e}}_s(t) . \quad (7)$$

where $\hat{\mathbf{v}}_s = [\hat{V}_{ds} \quad \hat{V}_{qs}]^T$.

At the next step $(k+1)$, the required command voltages $\hat{\mathbf{v}}_s^*(k)$ making the current $\mathbf{i}_s(k+1)$ be the command current $\mathbf{i}_s^*(k+1)$ can be derived from (7) as follows:

$$\hat{\mathbf{v}}_s^*(k) = R_s \mathbf{i}_s(k) + \sigma L_s \frac{[\mathbf{i}_s^*(k+1) - \mathbf{i}_s(k)]}{t_s} + \hat{\mathbf{e}}_s(t) \quad (8)$$

where $\hat{\mathbf{v}}_s^* = [\hat{V}_{ds}^* \quad \hat{V}_{qs}^*]^T$, t_s is a sampling time, and $\hat{\mathbf{v}}_s^*(k)$ and $\mathbf{i}_s^*(k+1)$ are the applied voltage and current command, respectively. This predictive current control block is shown in Fig. 3. If this optimal reference vector could be employed, the current error would always be nullified at the next time event. Since only the seven voltage vectors are available in practice in the RDCL inverter system, the next step is to find one of these nearest to the optimal reference vector as follows:

$$\mathbf{v}_s(k) = \begin{cases} V_0 & \text{if } |\hat{V}_s^*(k)| < \alpha \\ v_j^* & \text{if } |\hat{V}_s^*(k)| \geq \alpha \end{cases} \quad (9)$$

where $v_j^* = \left\{ v_j \in \mathbf{V} \;\middle|\; \min_{j \in J} [\,|\angle(v_j) - \angle(\hat{V}_r^*(k))|\,] \right\}$.

Note that v_j denotes the elements of the set of actual voltage vectors as $\mathbf{V} = \{v_j\} = \{V_1, V_2, V_3, V_4, V_5, V_6\}$ and the subscript "j" is defined as the ordering numbers indicating the elements of the set V sequentially. V_0 is a zero vector, constant α is dependent on the designer's choice. If a large α is chosen, the motor current response shows some phase delay because many zero vectors are employed. In Fig. 4, the required command voltage vector $\hat{V}_r^*$ and γ are calculated from $\hat{V}_{ds}^*$ and $\hat{V}_{qs}^*$ as follows:

$$|\hat{V}_r^*| = \sqrt{\hat{V}_{ds}^{*\,2} + \hat{V}_{qs}^{*\,2}} . \quad (11)$$

$$\theta = \angle \hat{V}_r^* = \tan\left(\frac{\hat{V}_{qs}^*}{\hat{V}_{ds}^*}\right) . \quad (12)$$

The overall block diagram of the speed control system employing the proposed current control technique is shown in Fig. 5. This proposed current control scheme is relatively simple compared with the modulation methodologies adopted for other current controlled inverter and can be easily realized with a full digital based hardware.

V. SIMULATION RESULTS

The proposed scheme is applied to the field oriented speed control system of a three phase induction machine. The proposed predictive current control technique, CRDM, and synchronized CRDM with hysteresis band are simulated as shown in Figs. 6 through 10, with full load T_{LOAD}=15.0 [N.m]. Assuming that the resonant DC link appears constant clamped sinusoidal waveforms with a period of 50 [usec] and zero voltage for 10[usec], and only one voltage pulse can be applied to the inverter for a sampling instant. The system parameters used in the simulation of the resonant DC link inverter driving an induction motor are shown as follows :

Induction Motor

Rated power : 5 hp, P = 4 : pole number
J = 0.02 [kg. cm], $L_s = L_r$ = 0.112 [H]
L_m = 0.107 [H], $R_s = R_r$ = 0.943 [Ω]
Resonant DC link frequency : 20 [KHz], 600 [V_{pp}]

As shown in Fig. 6, the conventional CRDM shows a high current ripple and offset current for a-phase current and current error under the full load are shown. As can be seen in this figure, when the CRDM current control without hysteresis band is used, much larger current ripple and offset current are appeared and there exists large current errors especially in the neighborhood of the positive and negative peaks of the current command. Fig. 7 shows the results of the synchronized CRDM with a hysteresis band of h=± 0.5[A]. Although a better control performance in view of the current ripple can be obtained using the synchronized CRDM technique with hysteresis band based on the space

vector PWM, the large current ripple is still exists. For the predictive current control, the current command, feedback current with $\alpha = 0.1 V_p$ are shown in Fig. 8 as well as the current error. As can be seen in this figure, the proposed control technique shows a nearly optimized response in view of the current ripple and offset. It can be therefore considered that the proposed predictive current control technique is very useful for a high performance induction motor control system based on an RDCL inverter. As can be seen in Figs. 9-10, torque and current transient responses show the reduced ripple and offset under the load torque variation. Under the variation of the load, the SCRDM shows less current ripple than the conventional CRDM for all ranges of load as shown in Fig. 11. The offset current of CRDM is increased as the load is increased and that of SCRDM is rather decreased as the load is increased as shown in Fig. 12. It is however shown in this figure that the proposed predictive current control is independent of the load change. The offset current and ripple of the predictive current control are greatly reduced than those of SCRDM and CRDM.

VI. CONCLUSION

A novel predictive current control technique is proposed in this paper as a new effective way of overcoming the disadvantages of the RDCL inverter based current control of an induction motor. Based on the discrete induction motor model, the optimal voltage vector minimizing the present current error is analytically calculated to apply the actual voltage vector. Using the proposed control technique, nearly optimum inverter voltages with respect to current ripple are obtained. Furthermore, the current offset is also notably reduced. Thus, the current ripple can be minimized and high performance of the torque and speed controls can also be available by the precise motor current control. The proposed current control technique is very useful for a high performance induction motor control system based on RDCL inverter.

NOMENCLATURE

R_s , R_r : Stator and rotor resistance

L_s , L_r : Stator and rotor inductance

L_m : mutual inductance

$\sigma = 1 - \dfrac{L_m^2}{L_s L_r}$: leakage coefficient

ω_r , ω_e : rotor and electrical angular speeds

$\tau_s = \dfrac{L_s}{R_s}$, $\tau_r = \dfrac{L_r}{R_r}$: stator and rotor time constant

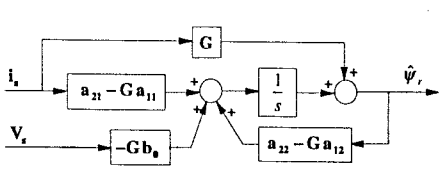

Fig. 1. Rotor flux observer.

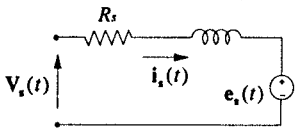

Fig. 2. Equivalent circuit of an induction motor.

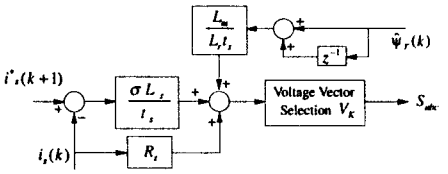

Fig. 3. Predictive current control block in discrete form.

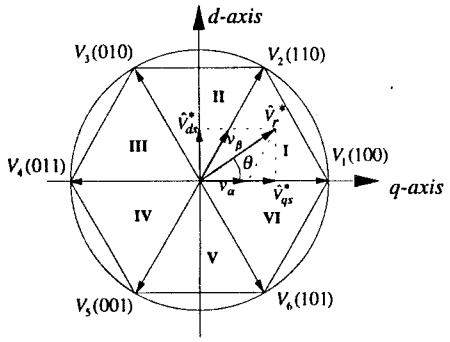

Fig. 4. Space voltage vectors in d-q frame.

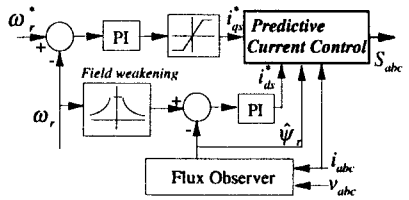

Fig. 5. Overall system control block diagram.

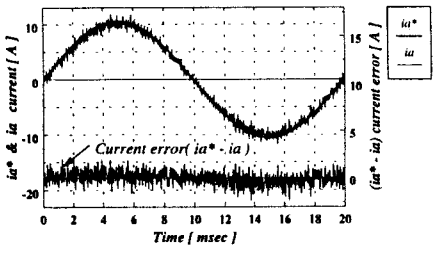

Fig. 6. Current command, feedback waveforms, and current error by the control of conventional CRDM inverter

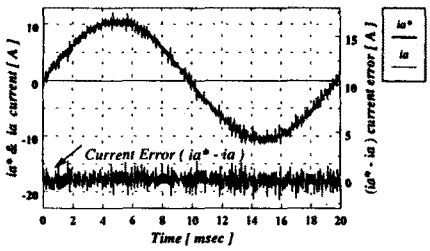

Fig. 7. Current command, feedback waveforms, and current error by the control of synchronized RLDC inverter with hysteresis band h = ±0.5[A].

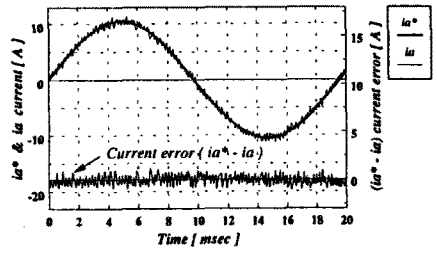

Fig. 8. Current command, feedback waveforms, and current error by the predictive current control using resonant link inverter.

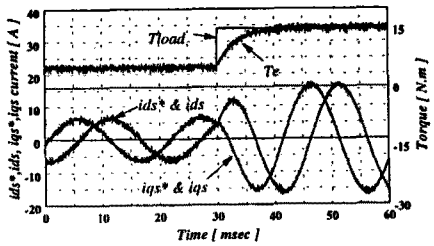

Fig. 9. i_{ds}, i_{qs}, load torque command, and developed torque transient curves by using the predictive current control.

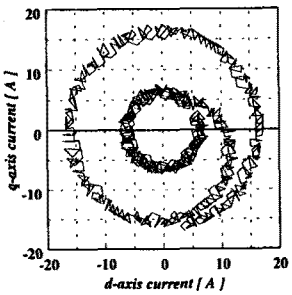

Fig. 10. i_{ds}, i_{qs} current trajectories in d-q frame for the load torque change from 5[N.m] to 15 [N.m].

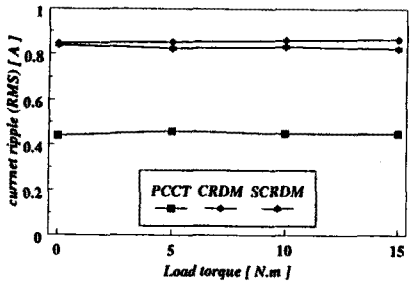

Fig. 11. Current ripple characteristics with load change for predictive current control technique (PCCT), CRDM, synchronized CRDM.

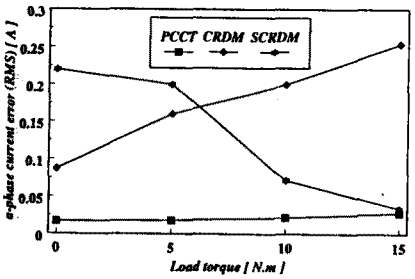

Fig. 12. Current offset characteristics with load change for predictive current control technique (PCCT), CRDM, synchronized CRDM.

VII. REFERENCE

[1] W.Y. and G. H. Cho, "Program-controlled soft switching PRDCL inverter with new space vector PWM algorithm", PESC, p314~319, 1992.

[2] Y. C. Jung and G. H. Cho, "Soft switching space vector PWM inverter using a new quasi-parallel resonant DC link", PESC, p936~941, 1995.

[3] K. Wang and F. C. Lee, "Novel DC-rail soft-switched three-phase voltage source inverters", IAS, p2610~2617, 1995.

[4] L. Malesani and V. Toigo, "High efficiency quasi-resonant DC link three-phase power inverter for full range PWM", Tran. on. Indus. Appl. Vol.3, No.1, 1995.

[5] D. M. Divan and L. Malesani, "A synchronized resonant DC link converter for soft-switched PWM",IEEE Trans. on Ind. Appl. , No. 5, Vol 29,pp940 ~948, 1993.

[6] Y. Hori and T. Umeno, "Implementation of robust observer based field orientation (FIFO) controller for induction machines", IAS, p523~528, 1989.

[7] L. B. Brahim and A. Kawamura, "Digital current regulation of field oriented controlled induction motor based on predictive flux observer", IAS, p607~612, 1990.

[8] T. G. Habetler and D. M. Divan, "Control strategies for direct torque control using discrete pulse modulation", IEEE Trans. on Indus. Appl. Vol-27, No. 5, 1991.

[9] G. Venkataramanan and D. M. Divan, "Improved performance voltage and current regulators using discrete pulse modulation", PESC., pp. 601-606, 1992.